Journal of Physics A: Mathematical and Theoretical

LETTER • OPEN ACCESS

Fractional Brownian motion in superharmonic potentials and non-Boltzmann stationary distributions

To cite this article: Tobias Guggenberger *et al* 2021 *J. Phys. A: Math. Theor.* **54** 29LT01

OPEN ACCESS
IOP Publishing

Letters
Journal of Physics A: Mathematical and Theoretical

J. Phys. A: Math. Theor. **54** (2021) 29LT01 (17pp) https://doi.org/10.1088/1751-8121/ac019b

Letter

Fractional Brownian motion in superharmonic potentials and non-Boltzmann stationary distributions

Tobias Guggenberger[1], Aleksei Chechkin[1,2] and Ralf Metzler[1,*]

[1] Institute of Physics & Astronomy, University of Potsdam, 14476 Potsdam-Golm, Germany
[2] Akhiezer Institute for Theoretical Physics, Kharkov 61108, Ukraine

E-mail: rmetzler@uni-potsdam.de

Received 23 February 2021, revised 22 April 2021
Accepted for publication 14 May 2021
Published 14 June 2021

Abstract

We study the stochastic motion of particles driven by long-range correlated fractional Gaussian noise (FGN) in a superharmonic external potential of the form $U(x) \propto x^{2n}$ ($n \in \mathbb{N}$). When the noise is considered to be external, the resulting overdamped motion is described by the non-Markovian Langevin equation for fractional Brownian motion. For this case we show the existence of long time, stationary probability density functions (PDFs) the shape of which strongly deviates from the naively expected Boltzmann PDF in the confining potential $U(x)$. We analyse in detail the temporal approach to stationarity as well as the shape of the non-Boltzmann stationary PDF. A typical characteristic is that subdiffusive, antipersistent (with negative autocorrelation) motion tends to effect an accumulation of probability close to the origin as compared to the corresponding Boltzmann distribution while the opposite trend occurs for superdiffusive (persistent) motion. For this latter case this leads to distinct bimodal shapes of the PDF. This property is compared to a similar phenomenon observed for Markovian Lévy flights in superharmonic potentials. We also demonstrate that the motion encoded in the fractional Langevin equation driven by FGN always relaxes to the Boltzmann distribution, as in this case the fluctuation-dissipation theorem is fulfilled.

*Author to whom any correspondence should be addressed.

Keywords: anomalous diffusion, Boltzmann distribution, non-Gaussian distribution

(Some figures may appear in colour only in the online journal)

1. Introduction

Robert Brown's vivid account on the 'rapid oscillatory motion' of what he called 'molecules' [1], micron-sized granules contained in the pollen grains of the flowering plant *Clarckia pulchella*[3], inspired the probabilistic theoretical formulations of diffusive processes by Einstein [2], Sutherland [3], and Smoluchowski [4]. A central idea of stochastic processes [5] was the concept of fluctuating forces [6, 7] originally formulated by Langevin in his description of 'Brownian motion' based on the extension of Newton's second law [8, 9]. Brownian motion as a mathematical model [10] soon emerged as a cornerstone of non-equilibrium statistical physics and physical kinetics [7, 11]. Notably, the theoretical predictions of Einstein, Sutherland, Smoluchowski, and Langevin were soon confirmed by experimentalists such as Perrin [12], Nordlund [13], and Kappler [14].

While normal Brownian diffusion is characterised by the linear time dependence of the mean squared displacement (MSD) $\langle X^2(t)\rangle = \int_{-\infty}^{\infty} x^2 P(x,t)\mathrm{d}x$, anomalous diffusion has the non-linear form $\langle X^2(t)\rangle \simeq K_\alpha t^\alpha$, with the anomalous diffusion exponent α and the generalised diffusion coefficient K_α of physical dimension $\mathrm{cm}^2/\mathrm{sec}^\alpha$. Depending on the value of α we distinguish subdiffusion ($0 < \alpha < 1$) and superdiffusion ($\alpha > 1$) [15, 16]. A wide range of observations of anomalous diffusion come from biological and soft matter systems [17–19]. Subdiffusion was reported for tracer motion in living cells [20–26] and in complex liquids [27–31]. Superdiffusion, based on active motion in living cells, was studied in [26, 32–36]. We also mention results for anomalous diffusion from supercomputing and experimental studies of membrane systems [37–43], internal protein dynamics [44, 45], or the motion along membranes and other surfaces [46–50].

As suggested by Einstein [2], normal diffusion with its linear time dependence of the MSD and the Gaussian probability density function (PDF) can be understood as resulting from a random motion consisting of a sequence of random displacements which satisfy the following three conditions: (i) there is a finite correlation time after which individual displacements become stochastically independent, (ii) the displacements are identically distributed, and (iii) the displacements have a finite second moment. Anomalous diffusion may appear whenever one of these conditions is violated [15, 16, 51]. We here consider the case when long-range temporal correlations of the displacements effect anomalous diffusion. The prototypical example for this mechanism is the Mandelbrot–van Ness fractional Brownian motion (FBM), a Gaussian, non-Markovian process with stationary increments [52, 53]. FBM has been identified to give rise to the anomalous-diffusive behaviour in a variety of systems including tracer motion in complex liquids [27, 28], in living cells [20, 24, 25, 54, 55] and in membrane dynamics [39, 40, 42]. FBM-like correlations are particularly studied in modern financial market models to account for market 'roughness' [56–58], and similar effects in network traffic [59]. FBM was also applied to describe observed density profiles of serotonergic brain fibres [60].

For many experimentally relevant scenarios it is important to study the behaviour of a stochastic motion under confinement. When this motion is normal Brownian diffusion, at long times the equilibrium state is characterised by the Boltzmann distribution, a fundamental property of statistical mechanics [61]. Thus, for a particle in a confining external potential

[3] Now renamed *Clarkia pulchella*.

$V(x)$, in the overdamped limit $\lim_{t\to\infty} P(x,t) = \mathcal{N}\exp(-\beta V(x))$, where $\beta = 1/[k_B T]$ is the Boltzmann factor and $\mathcal{N}$ a normalisation. Typically, the dynamical approach to this distribution from a non-equilibrium state is described by the Fokker–Planck–Smoluchowski equation [62]. Confinement can be induced when the tracer is measured in an optical tweezers setup, exerting a Hookean restoring force on the tracer [20, 28]. In internal protein dynamics relative motion of two aminoacids is effectively harmonically confined through the protein backbone connecting these aminoacids [44, 45], similar to the confinement of a tracer induced by a linker molecule [63]. Inside the cell, tracers are confined by the cell walls or internal membrane barriers. Growing serotonergic brain fibres are confined in specific brain regions [60].

To study confinement effects for systems driven by fractional Gaussian noise (FGN), one of the main frameworks is based on the Langevin equation for FBM and the fractional Langevin equation (FLE) introduced below. If we assume the validity of the fluctuation-dissipation theorem (FDT) [64], the system equilibrates to the stationary Boltzmann distribution and has a well-defined temperature. In this case, the driving FGN is called 'internal' and represents the 'bath' variables [7]. However, especially in biological systems the equilibrium assumption fails due to perpetual, energy-consuming active processes. Following Klimontovich the measured anomalous diffusion can be described by the Langevin equation driven by 'external' noise [65], which we here model by FGN. Recent numerical studies of the overdamped Langevin equation with reflecting boundary conditions and driven by FGN showed that the long-time stationary PDF deviates strikingly from the Boltzmann distribution, which in this case would be a uniform distribution [60, 66, 67]. In fact a similar situation is known for Markovian Lévy flights in a superharmonic potential $U(x) \propto x^{2n}$, $n \in \mathbb{N}$, which can be described by an overdamped Langevin equation driven by Lévy stable noise. It was shown that the long-time stationary PDF disagrees with the Boltzmann distribution even for the harmonic case [68, 69] and even features distinct bimodal and transient multimodal shapes despite the unimodal confining potential [70–73]. For the FLE the PDF for the free (no confining potential) and harmonic potential cases were obtained [74, 75]. The FLE has also been studied with reflecting boundary conditions and a flat potential with exponential confining 'wings' [76–78].

We here investigate numerically the diffusive motion of particles confined in a superharmonic external potential, based on the overdamped Langevin equation driven by FGN. We find that the stationary PDF deviates significantly from the naively expected Boltzmann distribution. Remarkably, the stationary PDF exhibits a distinct bimodal shape for steeper than harmonic potentials, despite the unimodal nature of the confining potential. The resemblance with results found for Lévy flights in superharmonic potential [70–73] is discussed. Finally we demonstrate that for the overdamped FLE the PDF converges to the Boltzmann distribution, as it should.

2. Fractional Brownian motion and fractional Gaussian noise

FBM is a centred Gaussian process with two-time auto-covariance function

$$\langle X(t_1)X(t_2)\rangle = K_\alpha\left[t_1^\alpha + t_2^\alpha - |t_1 - t_2|^\alpha\right], \quad 0 < \alpha \leqslant 2, \tag{1}$$

including the MSD $\langle X^2(t)\rangle = 2K_\alpha t^\alpha$ for $t_1 = t_2 = t$. For $\alpha = 1$ the correlations vanish, and FBM reduces to Brownian motion. The PDF of FBM for natural boundary conditions ($\lim_{|x|\to\infty} P(x,t) = 0$) is the Gaussian

$$P(x,t) = \frac{1}{\sqrt{4\pi K_\alpha t^\alpha}}\exp\left(-\frac{x^2}{4K_\alpha t^\alpha}\right). \tag{2}$$

Since the sample paths of FBM are almost surely continuous but not differentiable [52], we follow Mandelbrot and van Ness and define FGN as the difference quotient [52]

$$\xi(t;\delta t) = \frac{X(t+\delta t) - X(t)}{\delta t}, \tag{3}$$

where δt is a small but finite time step. It follows that FGN is a centred stationary Gaussian process whose auto-covariance function is readily obtained from (1) and (3),

$$\langle \xi(t;\delta t)\xi(t+\tau;\delta t)\rangle = K_\alpha(\delta t)^{\alpha-2}\left[\left|\frac{\tau}{\delta t}+1\right|^\alpha + \left|\frac{\tau}{\delta t}-1\right|^\alpha - 2\left|\frac{\tau}{\delta t}\right|^\alpha\right]. \tag{4}$$

The variance of FGN is thus $\langle \xi^2(t;\delta t)\rangle = 2K_\alpha(\delta t)^{\alpha-2}$. At times much longer than the time step, $\tau \gg \delta t$, one has[4]

$$\langle \xi(t;\delta t)\xi(t+\tau;\delta t)\rangle \sim K_\alpha\alpha(\alpha-1)\tau^{\alpha-2}, \tag{5}$$

and hence the correlations are positive (negative) for $\alpha > 1$ ($\alpha < 1$). Considering δt to be 'infinitesimally small' we write $\xi(t)$ and formally take it as the 'derivative' of FBM with covariance (5) ($\tau > 0$), so that $X(t) = \int_0^t \xi(t')\mathrm{d}t'$. Finally we mention that

$$\begin{aligned}\int_0^\infty \langle \xi(t;\delta t)\xi(t+\tau;\delta t)\rangle \mathrm{d}\tau &= K_\alpha(\delta t)^{\alpha-1}\left[\int_0^1 [(s+1)^\alpha + (1-s)^\alpha - 2s^\alpha]\,\mathrm{d}s\right.\\ &\quad \left. + \int_1^\infty [(s+1)^\alpha + (s-1)^\alpha - 2s^\alpha]\mathrm{d}s\right]\\ &= \frac{K_\alpha(\delta t)^{\alpha-1}}{\alpha+1}\lim_{s\to\infty}\left[(s+1)^{\alpha+1} + (s-1)^{\alpha+1} - 2s^{\alpha+1}\right]\\ &= \begin{cases} 0, & 0<\alpha<1\\ K_\alpha, & \alpha = 1\\ \infty, & 1<\alpha<2. \end{cases}\end{aligned} \tag{6}$$

Equations (5) and (6) demonstrate a drastic difference between persistent ($1 < \alpha < 2$) and antipersistent ($0 < \alpha < 1$) FGNs, in particular, note the vanishing integral over the noise auto-covariance.

2.1. Overdamped Langevin equation for FBM

The overdamped Langevin equation for a test particle performing FBM reads

$$\frac{\mathrm{d}X(t)}{\mathrm{d}t} = -\frac{1}{m\zeta}\frac{\mathrm{d}U}{\mathrm{d}x}(X(t)) + \xi(t), \qquad U(x) = \frac{k}{2n}x^{2n}, \tag{7}$$

where $X(t)$ is the particle position and $U(x)$ is the external potential, where $k > 0$ and $n \in \mathbb{N}$. This potential is harmonic for $n = 1$ and will be called 'superharmonic' for $n > 1$. The particle

[4] Using $(x \pm 1)^\alpha = \sum_{k=0}^\infty \frac{1}{k!}\frac{\mathrm{d}^k x^\alpha}{\mathrm{d}x^k}(\pm 1)^k$.

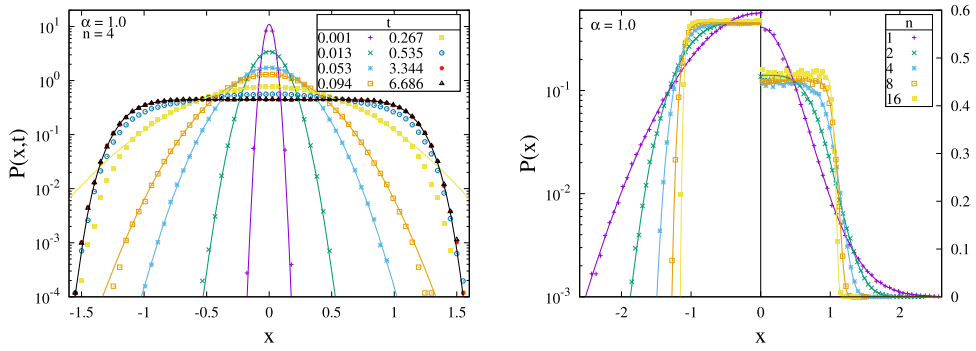

Figure 1. PDF for uncorrelated white Gaussian noise ($\alpha = 1$). Left: time evolution of the PDF for a superharmonic potential with $n = 4$. The black line shows the theoretical Boltzmann distribution (9), the coloured lines show the (rescaled) Gaussian (2) for free motion. Note the increasing deviation of the simulations from this short-time form, as it should be. Note that the 'strange' values for the time t arise due to the rescaling to dimensionless variables. Right: stationary PDF for different superharmonic potentials. The coloured lines show the Boltzmann distribution (9). For $x < 0$ the (symmetric) data is plotted logarithmically (left axis) and for $x \geqslant 0$ linearly (right axis).

is driven by the FGN $\xi(t)$, m is the mass of the particle and ζ is a friction coefficient of dimension $1/\text{sec}$. The Langevin equation (7) can be rewritten as

$$\frac{\mathrm{d}X(t)}{\mathrm{d}t} = -\frac{\mathrm{d}U}{\mathrm{d}x}(X(t)) + \eta(t), \qquad U(x) = \frac{x^{2n}}{2n}, \tag{8}$$

in dimensionless form, where $\eta(t) = \xi(t)/\sqrt{2K_\alpha}$ is a normalised FGN. The two relevant parameters defining our system are the anomalous diffusion exponent α and the power exponent n of the potential.

We note that the FGN in the Langevin equations (7) and (8) is external, i.e. the FDT is not fulfilled for $\alpha \neq 1$. Thus while for any process driven by a random force with finite variance a confining potential will lead to the emergence of a stationary PDF at long times, this will not be a thermalised Boltzmann distribution, see below. Only in the uncorrelated case ($\alpha = 1$), when the FGN is a white Gaussian unit noise, $\langle \eta(t_1)\eta(t_2)\rangle = \delta(t_1 - t_2)$ and hence the PDF $P(x, t)$ satisfies the Fokker–Planck-equation, the stationary state is given by the Boltzmann distribution. For the initial condition $P(x, 0) = \delta(x)$ it is straightforward to show that the stationary solution $P(x) = \lim_{t\to\infty} P(x, t)$ is the Boltzmann distribution

$$P(x) = \mathcal{N}_1(n) \exp\left(-\frac{x^{2n}}{n}\right), \qquad \mathcal{N}_1(n) = \frac{n^{1-1/(2n)}}{\Gamma\left(1/(2n)\right)}, \tag{9}$$

where $\Gamma(z) = \int_0^\infty s^{z-1}\mathrm{e}^{-s}\,\mathrm{d}s$ is the gamma function. Figure 1 shows simulations results for the time-dependent and stationary PDF for the Brownian case $\alpha = 1$. At short times the PDF is given by the (rescaled) Gaussian (2) for the free case, and it relaxes towards the Boltzmann PDF (9).

3. Results

3.1. Harmonic potential

For the harmonic potential ($n = 1$) the PDF $P(x,t)$ for FBM satisfies the Fokker–Planck equation [79]

$$\frac{\partial}{\partial t}P(x,t) = \frac{\partial}{\partial x}\left[xP(x,t)\right] + D(t)\frac{\partial^2}{\partial x^2}P(x,t), \tag{10}$$

with initial condition $P(x,0) = \delta(x)$ and the time-dependent coefficient

$$D(t) = \int_0^t \mathrm{e}^{-\tau}\langle\eta(t)\eta(t+\tau)\rangle \mathrm{d}\tau = \frac{\alpha}{2}\left(t^{\alpha-1}\,\mathrm{e}^{-t} + \gamma(\alpha,t)\right) \xrightarrow{t\to\infty} \frac{\Gamma(\alpha+1)}{2}, \tag{11}$$

where $\gamma(z,t) = \int_0^t s^{z-1}\,\mathrm{e}^{-s}\,\mathrm{d}s$ is the incomplete gamma function. The PDF has the Gaussian form and long time limit

$$P(x,t) = \frac{1}{\sqrt{2\pi\langle X^2(t)\rangle}}\exp\left(-\frac{x^2}{2\langle X^2(t)\rangle}\right) \xrightarrow{t\to\infty} \frac{1}{\sqrt{\pi\Gamma(\alpha+1)}}\exp\left(-\frac{x^2}{\Gamma(\alpha+1)}\right). \tag{12}$$

The MSD follows directly from the Langevin equation [75],

$$\langle X^2(t)\rangle = t^\alpha\,\mathrm{e}^{-t} + \frac{\gamma(\alpha+1,t)}{2} - \frac{t^{\alpha+1}\,\mathrm{e}^{-2t}}{2(\alpha+1)}M(\alpha+1,\alpha+2,t) \xrightarrow{t\to\infty} \frac{\Gamma(\alpha+1)}{2}, \tag{13}$$

in terms of the Kummer function $M(a,b,z)$ [80]. The explicit α-dependence in the stationary solution (12) and the corresponding stationary MSD (13) demonstrates the non-thermal character of FBM.

3.2. Superharmonic potential

As we have seen in the case of uncorrelated noise ($\alpha = 1$) as well as in the case of an harmonic potential ($n = 1$), the PDF converges at long times to the Boltzmannian

$$P(x) = \mathcal{N}_2\,\exp\left(-aU(x)\right), \tag{14}$$

with $a > 0$ and normalisation constant $\mathcal{N}_2$ [5]. One may expect that in the case of correlated Gaussian noise with a superharmonic potential ($\alpha \neq 1$, $n \geqslant 2$) the PDF still relaxes to the Boltzmannian, however, we will show that the actual form of the stationary PDF strongly deviates from the form (14).

Figure 2 shows simulation results for the time-dependent and stationary PDF in a quartic potential ($n = 2$). Note that in the ballistic limit $\alpha = 2$, for which the FGN becomes time-independent and perfectly correlated, one has $\int_0^t \eta(\tau)\mathrm{d}\tau = Zt$, where the amplitude Z is distributed like a unit Gaussian, $Z \overset{\mathrm{d}}{=} \mathcal{N}(0,1)$. Hence, in the ballistic limit, the randomness of the motion is solely due to a random 'initial velocity' Z.

At short times the PDF agrees with the (rescaled) Gaussian (2) in the free (unconfined) case. At long times the PDF converges to a stationary PDF that is significantly different from the

[5] For uncorrelated noise we have $a = 2$ and for correlated noise in the harmonic potential we have $a = 2/\Gamma(\alpha+1)$.

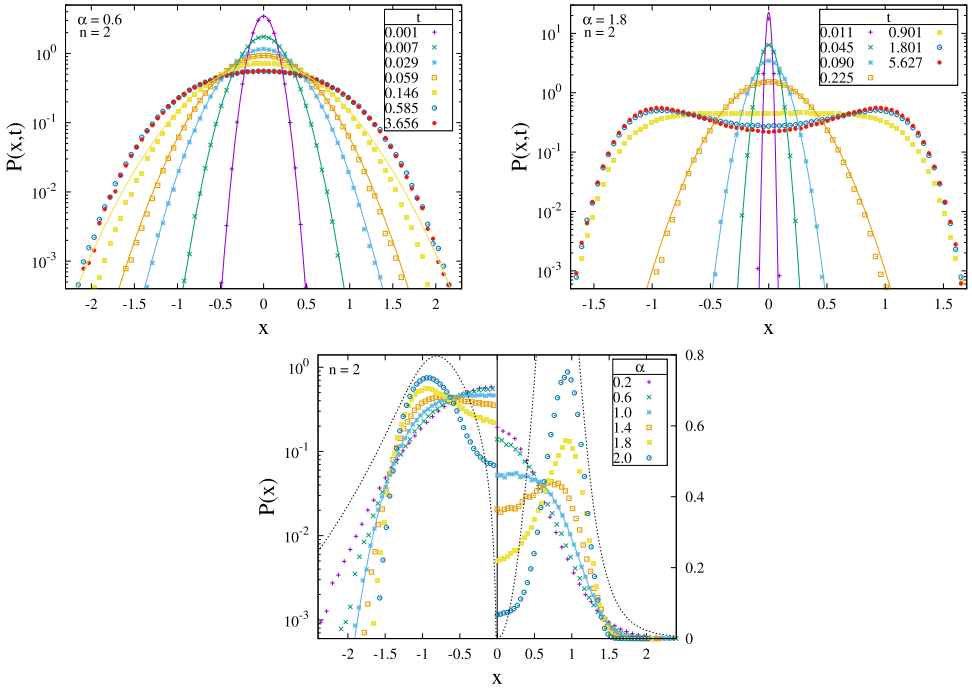

Figure 2. PDF for superharmonic potential with $n = 2$. Top: time dependence of PDFs for negatively ($\alpha = 0.6$, left) and positively ($\alpha = 1.8$, right) correlated FGN. The coloured lines show the corresponding (rescaled) Gaussian (2) of the free case. Bottom: stationary PDF for different values of α. The solid blue line represents the theoretical stationary PDF (9) for uncorrelated white Gaussian noise ($\alpha = 1$). The dashed line shows the curvature (15) of the potential. For $x < 0$ the data is plotted logarithmically (left axis) and for $x \geqslant 0$ linearly (right axis). For details of the numerical scheme see appendix A.

Boltzmannian (14). For positively correlated FGN ($\alpha > 1$) this difference is quite conspicuous, as the stationary PDF exhibits a distinct bimodal shape despite the unimodal and symmetric shape of the confining potential with a unique global minimum at the origin. Indeed, the stationary PDF has two global maxima located symmetrically with respect to the origin, and a local minimum at the origin. The amplitude of the two peaks increases with α, and the plot shows that their position is close to, but not exactly at the maxima of the curvature of the potential,

$$r(x) = \frac{|U''(x)|}{\left(1 + (U'(x))^2\right)^{3/2}} = \frac{(2n-1)x^{2n-2}}{\left(1 + x^{4n-2}\right)^{3/2}}. \tag{15}$$

For negatively correlated FGN ($\alpha < 1$) the difference of the stationary PDF to the Boltzmannian (14) is less obvious, as the PDF is still unimodal. We note that in figure 2 for $n = 2$ the tails of the stationary PDF decay progressively faster with increasing anomalous diffusion exponent α. This is in contrast to the harmonic case ($n = 1$) in which the tails of the PDF decay slower for increasing α, due to the dependence of the width $a = 2/\Gamma(\alpha + 1)$ in the corresponding Boltzmannian (14).

To analyse what controls the shape of the tails we computed the kurtosis κ of the simulated stationary PDFs that is defined as the fourth standardised moment

Table 1. Kurtosis κ of the simulated stationary PDFs in the quartic potential ($n = 2$), figure 2, for different anomalous diffusion exponents α. For uncorrelated noise ($\alpha = 1$) the value 2.19 expected for the Boltzmannian (14) is nicely reproduced. We also show the stretching exponent b (see equation (17)) for the unimodal subdiffusive cases, as extracted from the kurtosis κ. For the Brownian case ($\alpha = 1$) the expected value $b = 1$ is consistently recovered in this procedure.

α	κ	b
0.2	2.94	0.52
0.6	2.55	0.67
1.0	2.19	1.00
1.4	1.88	
1.8	1.56	

$\kappa = \langle (X - \langle X \rangle)^4 \rangle / \langle (X - \langle X \rangle)^2 \rangle^2$ and compare it to the kurtosis of the Boltzmannian (14),

$$\kappa = \Gamma\left(\frac{5}{2n}\right)\Gamma\left(\frac{1}{2n}\right) \Big/ \Gamma^2\left(\frac{3}{2n}\right). \tag{16}$$

For the harmonic potential ($n = 1$) the Boltzmannian is Gaussian with $\kappa = 3$ while for the quartic potential ($n = 2$) the Boltzmannian is 'super-Gaussian' with $\kappa \approx 2.19$. This platykurtic value means that the distribution falls off faster than a Gaussian normal distribution and thus has fewer and less extreme outliers. The crucial observation is that the kurtosis of the Boltzmannian only depends on n and not on a. Table 1 lists the kurtosis of the stationary PDFs for the quartic potential ($n = 2$) shown in figure 2. As can be seen, the kurtosis monotonically decreases with α. For the uncorrelated case ($\alpha = 1$) the kurtosis of the simulated data exactly reproduces the theoretical value $\kappa \approx 2.19$. For positively correlated FGN ($\alpha > 1$) the kurtosis values are smaller than this value, while for negatively correlated FGN ($\alpha < 1$) they are larger, in agreement with the observed faster or slower decay of the tails. We thus conclude that also for negatively correlated FGN ($\alpha < 1$) the stationary PDF is fundamentally different to the Boltzmannian (14).

As for negatively correlated FGN the monomodality of the PDF is preserved at all times but the shape is no longer Gaussian, it may be useful to have an empirical shape for the Boltzmannian. We propose the modified Gaussian (compare [40, 81])

$$P(x) = \mathcal{N}_2 \exp\left(-a[U(x)]^b\right), \tag{17}$$

with the normalisation $\mathcal{N}_2$ depending on the parameters $a > 0$ and $b > 0$ that in turn both may depend on n and α. For $b < 1$ this would correspond to a 'stretched' form as compared to the Boltzmann distribution (14) for the uncorrelated case ($\alpha = 1$), for which we have $b = 1$[6]. To validate this conjecture we fitted the modified Gaussian (17) to the simulated stationary PDF in the quartic potential ($n = 2$). Before fitting the parameter b was taken from table 1 for the corresponding kurtosis value, such that the only free parameter is a. This extracted value of b is also listed in table 1. The results shown in figure 3 on the left demonstrate that the empirical form (17) provides a quite accurate quantitative description of the stationary PDF. We note here that non-Gaussian shapes can be determined not only by the kurtosis. For the analysis of

[6] For positively correlated FGN ($\alpha > 1$) the stationary PDF cannot be of the shape (17) because of the observed bimodality.

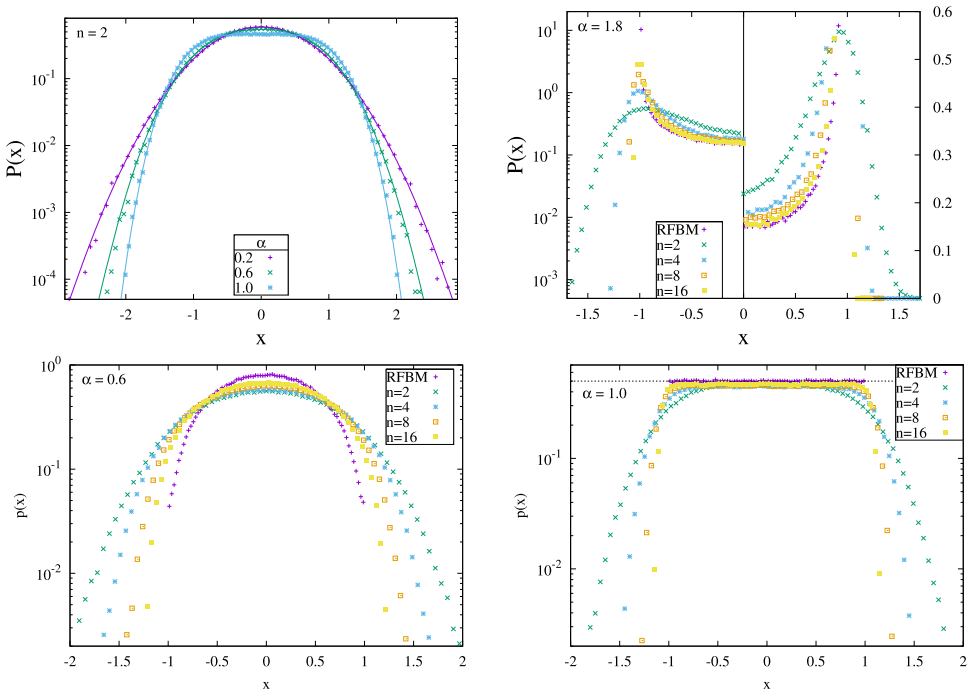

Figure 3. Top left: stationary PDF for the quartic potential with $n = 2$ and different subdiffusive exponents $\alpha < 1$ (negatively correlated FGN). The lines show fits with the function (17), where the fit parameter was a. The 'stretching' parameter b was fixed from the observed kurtosis value in table 1 by inverting the kurtosis formula (16) for the super-Gaussian. The case of normal diffusion ($\alpha = 1$) is shown for comparison. Top right: stationary PDF for $\alpha = 1.8$ and different superharmonic potentials. The data labelled 'RFBM' show the stationary PDF of reflected FBM in the interval $[-1, 1]$ [66]. For increasing n the potential approaches the box shape with infinite walls, and the stationary PDF clearly tends to the stationary PDF in the reflected case. Note that for $x < 0$ the data are plotted logarithmically (left axis) while for $x \geqslant 0$ they are plotted linearly (right axis). Bottom: plots of the stationary PDF along with the PDF for RFBM, for $\alpha = 0.6$ (left) and $\alpha = 1$ (right).

data deviations from a Gaussian can be determined from large-deviation analyses [82] or via the codifference [83].

Finally, figure 3 (right) shows the stationary PDF for different superharmonic potentials and compares them to the stationary PDF of reflected FBM, which was obtained numerically in [66]. As can be seen, the stationary PDF converges to the corresponding stationary PDF of reflected FBM in the interval $[-1, 1]$. This, of course, does not come as a surprize since for $n \to \infty$ the superharmonic potential converges to the infinite potential well in the interval $[-1, 1]$, in which the diffusing particle moves freely inside and is reflected at the borders. However, this convergence adds support to the claims in [66]: while for reflecting boundaries one may debate the correct implementation in the numerical scheme, for an external potential the stochastic description (7) appears fully natural.

3.3. Overdamped fractional Langevin equation motion

To demonstrate that the deviations from the Boltzmannian for FBM are due to the non-existence of the FDT, we briefly study the stationary PDF for the overdamped FLE [7, 74]. In our

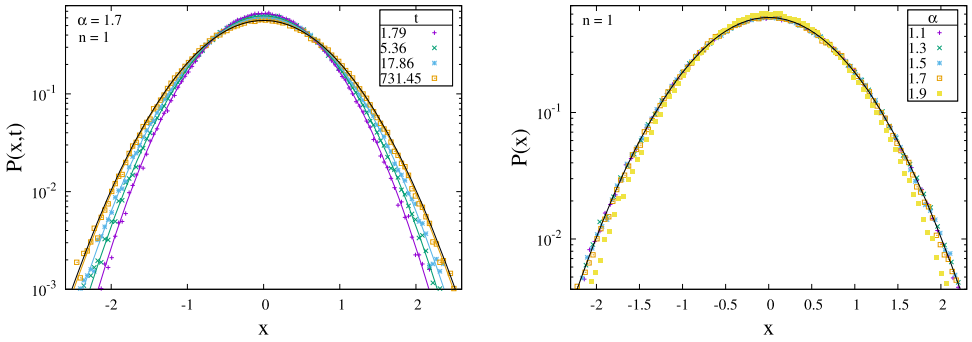

Figure 4. Time-dependent (left) and stationary (right) PDF for fractional Langevin equation motion in an harmonic potential ($n = 1$), for $x_0 = 0$. The coloured lines show the theoretical time-dependent PDF, a Gaussian with the second moment (21), the black line shows the stationary PDF $P(x) = \pi^{-1/2}\exp(-x^2)$.

dimensionless variables and for $1 < \alpha < 2$,

$$\alpha(\alpha-1)\int_0^t (t-t')^{\alpha-2}\frac{\mathrm{d}X(t')}{\mathrm{d}t'}\mathrm{d}t' + \frac{\mathrm{d}U}{\mathrm{d}x}(X(t)) = \eta(t), \tag{18}$$

where $\eta(t)$ is a normalised FGN and $U(x) = x^{2n}/(2n)$. Here the friction term includes a power-law memory that is coupled to the noise autocorrelation via the FDT $\langle\eta(t_1)\eta(t_2)\rangle = k(t_1 - t_2)/2$, where the memory kernel is $k(t-t') = \alpha(\alpha-1)(t-t')^{\alpha-2}$. The integral on the left-hand side of (18) can be interpreted as a fractional differential operator, therefore the name FLE [84]. The equilibrium Boltzmann distribution encoded in this equation for the superharmonic potential $U(x)$ is given by equation (9) with the equilibrium second moment

$$\langle X^2\rangle = \frac{n^{1/n}\Gamma(3/(2n))}{\Gamma(1/(2n))}. \tag{19}$$

For the harmonic potential ($n = 1$) the overdamped FLE can be solved analytically [74, 85]. The result is a Gaussian, that is fully characterised by the first two moments

$$\langle X(t)\rangle = x_0 E_{2-\alpha}\left(-\frac{t^{2-\alpha}}{\Gamma(1+\alpha)}\right), \tag{20}$$

and

$$\langle X^2(t)\rangle = \frac{1}{2} + \left(x_0^2 - \frac{1}{2}\right)E_{2-\alpha}^2\left(-\frac{t^{2-\alpha}}{\Gamma(1+\alpha)}\right). \tag{21}$$

Here we introduced the Mittag-Leffler function, that has the series expansions around zero and infinity [86]

$$E_\lambda(-z) = \sum_{\nu=0}^{\infty}\frac{(-1)^\nu z^\nu}{\Gamma(1+\lambda\nu)} \sim \sum_{\nu=1}^{N}\frac{(-1)^{\nu-1}}{\Gamma(1-\lambda\nu)z^\nu} + O\left(\frac{1}{z^{N+1}}\right), \quad z\in\mathbb{R}^+ \tag{22}$$

In our dimensionless variables the second moment has the stationary value $\langle X^2\rangle = 1/2$, such that the stationary PDF reaches the Gaussian Boltzmann form $P(x) = \pi^{-1/2}\exp(-x^2)$. Figure 4 shows the time-dependent PDF for $\alpha = 1.7$ and the stationary PDF for different α. Both for

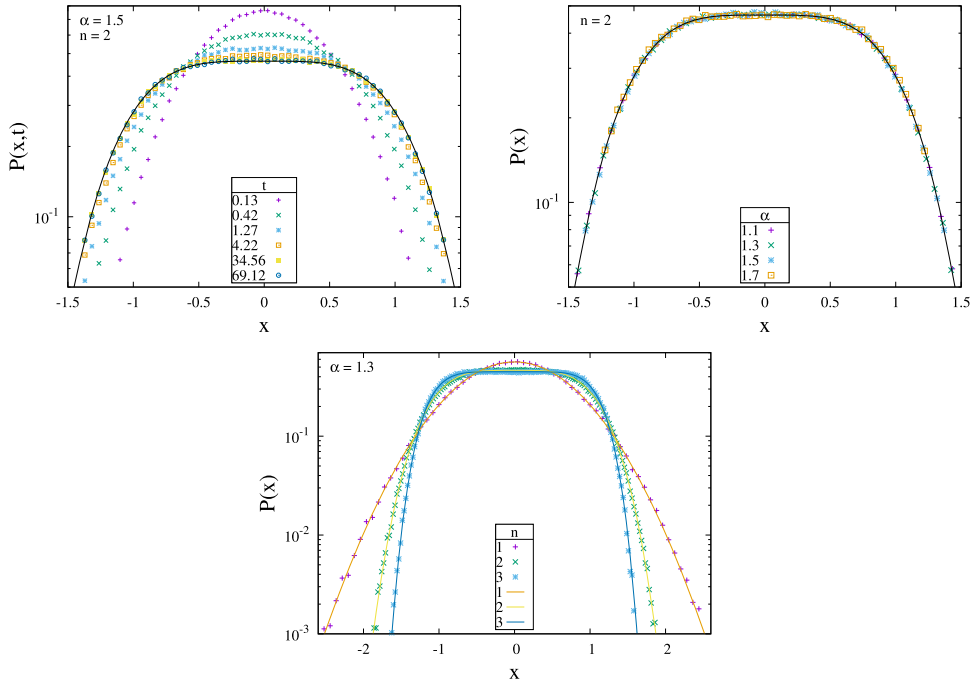

Figure 5. Top: time-dependent (left) and stationary (right) PDF for fractional Langevin equation motion in the quartic potential ($n = 2$). Bottom: Stationary PDF for $\alpha = 1.3$ and different superharmonic potentials. The lines show the (corresponding) Boltzmann equilibrium PDF (9), demonstrating excellent agreement.

the time-dependent and the stationary PDFs we see very good agreement with the predicted Gaussian forms. The slight deviation from the theoretical stationary PDF for the two largest α-values is due to the fact that stationarity was not fully reached at the maximal simulation time.

Figure 5 shows the time-dependent PDF for $\alpha = 1.5$ and the stationary PDF for different α for the quartic potential with $n = 2$ as well as the stationary PDF for $\alpha = 1.3$ and different superharmonic potentials. The PDF stays unimodal in all cases and the stationary PDF agrees very well with the Boltzmann distribution (9).

4. Conclusion

We studied FBM in steeper than harmonic external potentials on the basis of the overdamped Langevin equation driven by long-range correlated FGN. Our central finding is that the stationary PDF for this non-thermalised process significantly deviates from the naively expected Boltzmann form. Notably, for the positively correlated case we obtain a bimodal stationary PDF for steeper than harmonic external potentials. The maxima were shown to be located in close vicinity of the maximal potential curvature. As shown by the kurtosis the obtained stationary PDF decays faster than the Boltzmannian for the case of uncorrelated white Gaussian noise. For negatively correlated FGN the PDF remains monomodal but the tails decay slower than those of the Boltzmann form. In the latter case we showed that the observed stationary PDF is consistent with the empirical form $P(x) \propto \exp(-a[U(x)]^b)$, where the 'stretching' exponent

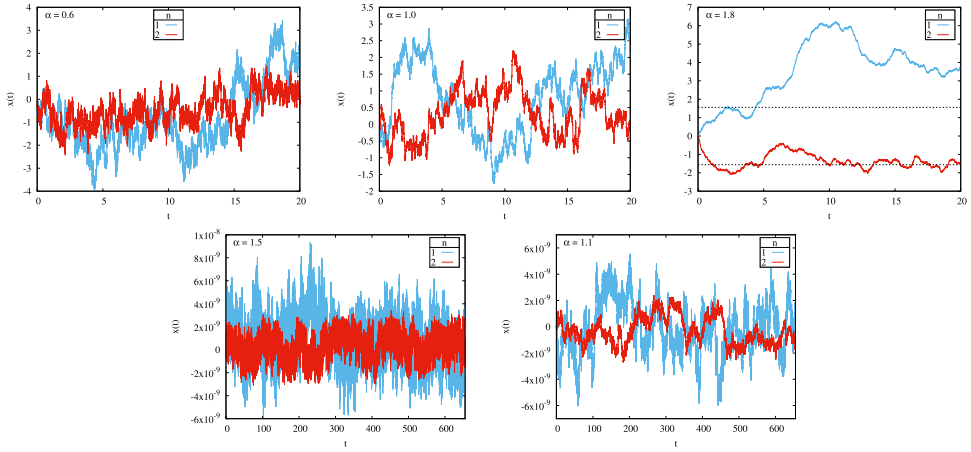

Figure 6. Sample trajectories in confining potentials in-dimensional units. Top row: FBM trajectories in harmonic ($n = 1$) and quartic ($n = 2$) potentials for $\alpha = 0.6$, $\alpha = 1.0$, and $\alpha = 1.8$ (left to right). In the panel for $\alpha = 1.8$ the dashed lines denote the location of the two maxima of the PDF for $n = 2$. Bottom row: FLE trajectories in harmonic ($n = 1$) and quartic ($n = 2$) potentials for $\alpha = 1.5$ and $\alpha = 1.1$. Note that for FLE motion $\alpha = 1.1$ and $\alpha = 1.5$ translates into subdiffusive motion with MSD exponent 0.9 and 0.5, respectively.

b was determined from the kurtosis value. Choosing increasingly steep external potentials we also demonstrated that the PDF in the long time limit converges to the non-uniform shapes obtained for reflected FBM in a box potential in [66].

For comparison we briefly consider the sample trajectories of the different confined dynamics considered herein. Figure 6 shows trajectories for both FBM and FLE motion in harmonic ($n = 1$) and quartic ($n = 2$) potentials, for different scaling exponents α of the FGN. For clarity we here use dimensional units for time t and position x, such that the stronger confinement in the quartic potential is visible. For FBM (top row in figure 6) the antipersistence of the motion for the subdiffusive case $\alpha = 0.6$ is in distinct contrast to the persistent behaviour for $\alpha = 1.8$. In the former case the particle rarely ventures deep into the potential well and has many zero-crossings. In the latter case the particle 'pushes' against one flank of the confining potential for considerable time spans. This effect is clearly seen in the top right panel of figure 6 for the case $n = 2$, as the trajectory wiggles around one of the two dashed lines representing the two maxima of the corresponding stationary PDF. The case of normal diffusion with $\alpha = 1.0$ is shown for comparison. FLE motion under confinement is shown in the bottom row for two α. We note that for FLE the short time expansion of the MSD (21) and $x_0 = 0$ reads $\langle X^2(t)\rangle \sim t^{2-\alpha}/\Gamma(1+\alpha)$. For $1 < \alpha < 2$ the motion is thus subdiffusive, and due to the FDT a higher α value leads to more pronounced antipersistence. As one can see, the qualitative behaviour between the subdiffusive FBM and FLE motion dynamics is not overly distinct from the trajectories, such that the assessment about the convergence to an equilibrated Boltzmann distribution is better visible in the PDFs of the processes.

We also remark that the bimodal shape of the stationary PDF for positive correlated noise observed here resembles the bimodal shapes for Lévy flights in superharmonic potentials reported in [70–73]. These Lévy flights are described by a Markovian Langevin equation driven by white yet Lévy stable noise. In this case the stationary distribution in the harmonic case is not a Boltzmann distribution but a Lévy stable density [68]. The bimodality of the PDF in

the case of Lévy flights emerges due to the strongly non-local jumps in space, characterised by the divergence of the variance of the jump lengths. As shown here, for the PDF the strong temporal persistence of superdiffusive FBM effects a similar bimodality. We also mention that the stationary distribution of the end point of a grafted, semi-flexible polymer was shown to have a bimodal distribution, where the degree of bimodality can be tuned by the stiffness of the polymer [87].

For FBM in an external potential the noise is viewed as 'external', and the system is not thermalised. This approach is often used in systems such as living biological cells, in which energy-consuming active processes drive the environment far from equilibrium. In contrast, when the system is thermalised and governed by an FDT the driving FGN is coupled to the velocity of the particle by a power-law memory kernel, described by the overdamped FLE. In this case the stationary distribution must be given by the Boltzmann distribution, as we confirmed for steeper than harmonic potentials.

Data availability statement

No new data were created or analysed in this study.

Acknowledgments

We acknowledge funding from the German Research Foundation (DFG) through Grant Number ME 1535/12-1. RM acknowledges the Foundation for Polish Science (Fundacja na rzecz Nauki Polskiej, FNP) for support in terms of an Alexander von Humboldt Honorary Polish Research Scholarship.

Appendix A. Numerics

We here discuss the numerical schemes to compute approximate solutions of the overdamped Langevin and the FLE discussed in the main text. The simulation of sample trajectories requires the simulation of sample times series of FBM and its increment process, which is briefly discussed first. In the following we employ an equidistant time discretisation $t_i = i\delta t$ $(i = 0, \ldots, I)$ with time step $\delta t = t/I$ and maximal simulation time t.

Let $B(t)$ be a (normalised) FBM, $B(t) = \int_0^t \eta(\tau)\mathrm{d}\tau$ with (normalised) FGN $\eta(t)$. The time-discrete FBM $B_i = B(t_i) = B(i\delta t)$ then fulfils the recursion relation

$$B_0 = 0, \qquad B_i = B_{i-1} + R_{i-1}, \tag{A.1}$$

where $R_i = B_{i+1} - B_i$ are the increments of FBM with time step δt. This increment process is a centred Gaussian process with auto-covariance function $\langle R_i R_{i+j}\rangle = (\delta t^\alpha/2)(|j+1|^\alpha + |j-1|^\alpha - 2|j|^\alpha)$. We generated time-discrete increment sample trajectories by use of the Hosking method [88]. Time-discrete FBM sample trajectories were then generated via the recursion relation (A.1).

To obtain a numerical scheme for the (dimensionless) overdamped Langevin equation with superharmonic potential $U(x) = x^{2n}/(2n)$ we first integrate from t_{i-1} to t_i and obtain

$$X(t_i) = X(t_{i-1}) - \int_{t_{i-1}}^{t_i} X^{2n-1}(t')\mathrm{d}t' + [B(t_i) - B(t_{i-1})]. \tag{A.2}$$

With the (left) rectangle-rule $\int_{t_{i-1}}^{t_i} f(t')\mathrm{d}t' \approx \delta t f(t_{i-1})$ to approximate the integral in (A.2) we find for the following recursion relation for the numerical solution $\hat{X}_i \approx X(t_i)$,

$$\hat{X}_0 = X(0), \qquad \hat{X}_i = \hat{X}_{i-1} - \delta t \hat{X}_{i-1}^{2n-1} + R_{i-1}. \tag{A.3}$$

Now we turn to the (dimensionless) overdamped FLE with superharmonic potential. We rewrite it in the integral form

$$\int_0^t X^{2n-1}(t')\mathrm{d}t' = -\alpha(\alpha-1)\int_0^t (t-t')^{\alpha-2}X(t')\mathrm{d}t' + \alpha x_0 t^{\alpha-1} + B(t). \tag{A.4}$$

We approximate the integral on the left-hand side using the composite trapezoidal-rule

$$\int_0^{t_i} f(t')\mathrm{d}t' \approx \frac{\delta t}{2}[f(0)+f(t_i)] + \delta t \sum_{j=1}^{i-1} f(t_j). \tag{A.5}$$

The memory integral on the right-hand side is approximated by use of the formula [89]

$$\int_0^{t_i} (t_i - t')^{\alpha-2} f(t')\mathrm{d}t' \approx \frac{(\delta t)^{\alpha-1}}{\alpha(\alpha-1)} \sum_{j=0}^{i} a_{j,i} f(t_j), \tag{A.6}$$

where $\alpha > 1$ and

$$a_{j,i} = \begin{cases} (i-1)^\alpha - (i-\alpha)i^{\alpha-1}, & j = 0 \\ (i-j+1)^\alpha + (i-j-1)^\alpha - 2(i-j)^\alpha, & 1 \leqslant j \leqslant i-1. \\ 1, & j = i \end{cases} \tag{A.7}$$

We then obtain the implicit recursion relation for the approximate solution $\hat{X}_i \approx X(t_i)$,

$$\hat{X}_0 = x_0, \qquad 0 = \hat{X}_i^{2n-1} + a\hat{X}_i + d_i + c_i - \frac{2}{\delta t} B_i, \tag{A.8}$$

with $a = 2(\delta t)^{\alpha-2}$ and

$$d_i = 2\sum_{j=1}^{i-1} \hat{X}_j^{2n-1} + a\sum_{j=1}^{i-1} a_{j,i}\hat{X}_j, \qquad c_i = x_0^{2n-1} + x_0 a\left(a_{0,i} - \alpha i^{\alpha-1}\right) \tag{A.9}$$

and initial condition $x_0 = X(0)$. We solved the implicit recursion relation (A.8) numerically by use of Newton's method. To that end we define the function $f(y) = c_i - \frac{2}{\delta t}B_i + d_i + ay + y^{2n-1}$. We want to find z such that $f(z) = 0$ (i.e. $z = \hat{X}_i$). Given an initial guess z_0, Newton's method solves for z recursively via $z_{k+1} = z_k - f(z_k)/f'(z_k)$ with $k = 0, 1, \ldots$, and where f' denotes the derivative of f. Hence,

$$z_{k+1} = z_k - \frac{c_i - \frac{2}{\delta t}B_i + d_i + az_k + z_k^{2n-1}}{a + (2n-1)z_k^{2n-2}}. \tag{A.10}$$

To obtain an initial guess $z_0 = \hat{X}_i^{\mathrm{ini}}$, we approximate the integral on the left-hand side of the overdamped FLE not by the composite trapezoidal-rule (A.5) but by the composite (left)

rectangle-rule

$$\int_0^{t_i} f(t')\mathrm{d}t' \approx \delta t \sum_{j=0}^{i-1} f(t_j). \tag{A.11}$$

This leads to

$$z_0 = \hat{X}_i^{\mathrm{ini}} = \frac{1}{a}\left(-x_0^{2n-1} - d_i - c_i + \frac{2}{\delta t}B_i\right). \tag{A.12}$$

Equations (A.8), (A.10) and (A.12) were used for the computation of the sample trajectories.

ORCID iDs

Ralf Metzler https://orcid.org/0000-0002-6013-7020

References

[1] Brown R 1828 *Phil. Mag.* **4** 161
[2] Einstein A 1905 *Ann. Phys., Lpz.* **322** 549
[3] Sutherland W 1905 *Phil. Mag.* **9** 781
[4] von Smoluchowski M 1906 *Ann. Phys., Lpz.* **326** 756
[5] van Kampen N 1981 *Stochastic Processes in Physics and Chemistry* (Amsterdam: North-Holland)
[6] Brenig W 1989 *Statistical Theory of Heat: Nonequilibrium Phenomena* (Berlin: Springer)
[7] Zwanzig R 2001 *Nonequilibrium Statistical Mechanics* (Oxford: Oxford University Press)
[8] Langevin P 1908 *C. R. Acad. Sci., Paris* **146** 530
[9] Coffey W and Kalmykov Y P 2017 *The Langevin Equation: With Applications to Stochastic Problems in Physics, Chemistry and Electrical Engineering* (Singapore: World Scientific)
[10] Lévy P 1965 *Processus stochastiques et mouvement brownien* (Paris: Gauthier-Villars)
[11] Landau L D and Lifshitz E M 1981 *Physical Kinetics* (Oxford: Heinemann)
[12] Perrin J 1908 *C. R. Acad. Sci., Paris* **146** 967
[13] Nordlund I 1914 *Z. Phys. Chem.* **87** 40
[14] Kappler E 1931 *Ann. Phys., Lpz.* **403** 233
[15] Bouchaud J-P and Georges A 1990 *Phys. Rep.* **195** 127
[16] Metzler R and Klafter J 2000 *Phys. Rep.* **339** 1
[17] Norregaard K, Metzler R, Ritter C M, Berg-Sørensen K and Oddershede L B 2017 *Chem. Rev.* **117** 4342
[18] Höfling F and Franosch T 2013 *Rep. Prog. Phys.* **76** 046602
[19] Barkai E, Garini Y and Metzler R 2012 *Phys. Today* **65** 29
[20] Jeon J H, Tejedor V, Burov S, Barkai E, Selhuber-Unkel C, Berg-Sørensen K, Oddershede L and Metzler R 2011 *Phys. Rev. Lett.* **106** 048103
[21] Weiss M, Elsner M, Kartberg F and Nilsson T 2004 *Biophys. J.* **87** 3518
[22] Bronstein I, Israel Y, Kepten E, Mai S, Shav-Tal Y, Barkai E and Garini Y 2009 *Phys. Rev. Lett.* **103** 018102
[23] Burnecki K, Kepten E, Janczura J, Bronshtein I, Garini Y and Weron A 2012 *Biophys. J.* **103** 1839
[24] Weber S C, Spakowitz A J and Theriot J A 2010 *Phys. Rev. Lett.* **104** 238102
[25] Tabei S M A, Burov S, Kim H Y, Kuznetsov A, Huynh T, Jureller J, Philipson L H, Dinner A R and Scherer N F 2013 *Proc. Natl Acad. Sci.* **110** 4911
[26] Caspi A, Granek R and Elbaum M 2000 *Phys. Rev. Lett.* **85** 5655
[27] Szymanski J and Weiss M 2009 *Phys. Rev. Lett.* **103** 038102
[28] Jeon J-H, Leijnse N, Oddershede L B and Metzler R 2013 *New J. Phys.* **15** 045011
[29] Wong I Y, Gardel M L, Reichman D R, Weeks E R, Valentine M T, Bausch A R and Weitz D A 2004 *Phys. Rev. Lett.* **92** 178101

[30] Levin M, Bel G and Roichman Y 2020 arXiv:2011.00539
[31] Banks D S and Fradin C 2005 *Biophys. J.* **89** 2960
[32] Reverey J F, Jeon J H, Bao H, Leippe M, Metzler R and Selhuber-Unkel C 2015 *Sci. Rep.* **5** 11690
[33] Seisenberger G, Ried M U, Endreß T, Büning H, Hallek M and Bräuchle C 2001 *Science* **294** 1929
[34] Chen K, Wang B and Granick S 2015 *Nat. Mater.* **14** 589
[35] Song M S, Moon H C, Jeon J H and Park H Y 2018 *Nat. Commun.* **9** 344
[36] Thapa S, Lukat N, Selhuber-Unkel C, Cherstvy A G and Metzler R 2019 *J. Chem. Phys.* **150** 144901
[37] Weigel A V, Simon B, Tamkun M M and Krapf D 2011 *Proc. Natl Acad. Sci.* **108** 6438
[38] Weigel A V, Tamkun M M and Krapf D 2013 *Proc. Natl Acad. Sci.* **110** E4591
[39] Jeon J H, Monne H M S, Javanainen M and Metzler R 2012 *Phys. Rev. Lett.* **109** 188103
[40] Jeon J H, Javanainen M, Martinez-Seara H, Metzler R and Vattulainen I 2016 *Phys. Rev.* X **6** 021006
[41] He W, Song H, Su Y, Geng L, Ackerson B J, Peng H B and Tong P 2016 *Nat. Commun.* **7** 11701
[42] Kneller G R, Baczynski K and Pasenkiewicz-Gierula M 2011 *J. Chem. Phys.* **135** 141105
[43] Gupta S, de Mel J U, Perera R M, Zolnierczuk P, Bleuel M, Faraone A and Schneider G J 2018 *J. Phys. Chem. Lett.* **9** 2956
[44] Hu X, Hong L, Smith M D, Neusius T, Cheng X and Smith J C 2016 *Nat. Phys.* **12** 171
[45] Lu H P, Xun L and Xie X S 1998 *Science* **282** 1877
[46] Díez Fernández A, Charchar P, Cherstvy A G, Metzler R and Finnis M W 2020 *Phys. Chem. Chem. Phys.* **22** 27955
[47] Tan P, Liang Y, Xu Q, Mamontov E, Li J, Xing X and Hong L 2018 *Phys. Rev. Lett.* **120** 248101
[48] Yamamoto E, Kalli A C, Akimoto T, Yasuka K and Sansom M S P 2015 *Sci. Rep.* **5** 18245
[49] Krapf D, Campagnola G, Nepal K and Peersen O B 2016 *Phys. Chem. Chem. Phys.* **18** 12633
[50] Krapf D and Metzler R 2019 *Phys. Today* **72** 48
[51] Metzler R, Jeon J-H, Cherstvy A G and Barkai E 2014 *Phys. Chem. Chem. Phys.* **16** 24128
[52] Mandelbrot B B and Van Ness J W 1968 *SIAM Rev.* **10** 422
[53] Qian H 2003 Fractional Brownian motion and fractional Gaussian noise *Processes with Long-Range Correlations* (Berlin: Springer)
[54] Magdziarz M, Weron A, Burnecki K and Klafter J 2009 *Phys. Rev. Lett.* **103** 180602
[55] Krapf D *et al* 2019 *Phys. Rev.* X **9** 011019
[56] El Euch O and Rosenbaum M 2016 *Math. Finance* **29** 3
[57] Rostek S and Schöbel R 2013 *Econ. Modell.* **30** 30
[58] Comte F and Renault E 1998 *Math. Finance* **8** 291
[59] Mikosch T, Resnick S, Rootzén H and Stegeman A 2002 *Ann. Appl. Probab.* **12** 23
[60] Janušonis S, Detering N, Metzler R and Vojta T 2020 *Front. Comput. Neurosci.* **14** 56
[61] Landau L D and Lifshitz E M 1980 *Statistical Physics Part 1* (Oxford: Heinemann)
[62] Risken H 1989 *The Fokker–Planck Equation* (Berlin: Springer)
[63] Tolić-Nørrelykke S F, Rasmussen M B, Pavone F S, Berg-Sørensen K and Oddershede L B 2006 *Biophys. J.* **90** 3694
[64] Kubo R 1966 *Rep. Prog. Phys.* **29** 255
[65] Klimontovich Y L 1995 *Statistical Theory of Open Systems A Unified Approach to Kinetic Description of Processes in Active Systems* vol 1 (Berlin: Springer)
[66] Guggenberger T, Pagnini G, Vojta T and Metzler R 2019 *New J. Phys.* **21** 022002
[67] Vojta T, Halladay S, Skinner S, Janušonis S, Guggenberger T and Metzler R 2020 *Phys. Rev.* E **102** 032108
[68] Jespersen S, Metzler R and Fogedby H C 1999 *Phys. Rev.* E **59** 2736
[69] Chechkin A V and Gonchar V Y 2000 *J. Exp. Theor. Phys.* **91** 635
[70] Chechkin A, Gonchar V, Klafter J, Metzler R and Tanatarov L 2002 *Chem. Phys.* **284** 233
[71] Chechkin A V, Klafter J, Gonchar V Y, Metzler R and Tanatarov L V 2003 *Phys. Rev.* E **67** 010102
[72] Chechkin A V, Gonchar V Y, Klafter J, Metzler R and Tanatarov L V 2004 *J. Stat. Phys.* **115** 1505
[73] Capała K, Padash A, Chechkin A V, Shokri B, Metzler R and Dybiec B 2020 *Chaos* **30** 123103
[74] Kou S C 2008 *Ann. Appl. Stat.* **2** 501
[75] Jeon J H and Metzler R 2012 *Phys. Rev.* E **85** 021147
[76] Jeon J H and Metzler R 2010 *Phys. Rev.* E **81** 021103
[77] Holmes W R 2019 *Biophys. J.* **116** 1538
[78] Vojta T, Skinner S and Metzler R 2019 *Phys. Rev.* E **100** 042142
[79] Adelman S A 1976 *J. Chem. Phys.* **64** 124
[80] Abramowitz M and Stegun I A 1972 *Handbook of Mathematical Functions* (New York: Dover)
[81] Cherstvy A G, Nagel O, Beta C and Metzler R 2018 *Phys. Chem. Chem. Phys.* **20** 23034

[82] Thapa S, Wyłomańska A, Sikora G, Wagner C E, Krapf D, Kantz H, Chechkin A V and Metzler R 2021 *New J. Phys.* **23** 013008
[83] Ślęzak J, Metzler R and Magdziarz M 2019 *New J. Phys.* **21** 053008
[84] Lutz E 2001 *Phys. Rev.* E **64** 051106
[85] Kursawe J, Schulz J and Metzler R 2013 *Phys. Rev.* E **88** 062124
[86] Gorenflo R, Kilbas A A, Mainardi F and Rogosin R 2014 *Mittag-Leffler Functions, Related Topics and Applications* (Berlin: Springer)
[87] Benetatos P and Frey E 2005 *Phys. Rev.* E **72** 030801(R)
[88] Dieker T 2004 Simulation of fractional Brownian motion *Master's Thesis* Vrije Universiteit Amsterdam (revised version)
[89] Diethelm K, Ford N J and Freed A D 2002 *Nonlinear Dyn.* **29** 3